Biology Contribution

Effects of Single-Dose Versus Hypofractionated Focused Radiation on Vertebral Body Structure and Biomechanical Integrity: Development of a Rabbit Radiation-Induced Vertebral Compression Fracture Model

Alexander Perdomo-Pantoja, MD,* Christina Holmes, PhD,[†]
Ioan A. Lina, MD,[‡] Jason A. Liauw, MD,* Varun Puvanesarajah, MD,[§]
Brian C. Goh, MD, PhD,[‖] Chukwuebuka C. Achebe, BS,[¶]
Ethan Cottrill, MS,* Benjamin D. Elder, MD, PhD,[#]
Warren L. Grayson, PhD,[¶] Kristin J. Redmond, MD, MPH,**
Soojung C. Hur, PhD,[††] and Timothy F. Witham, MD*

*Department of Neurosurgery, Johns Hopkins University School of Medicine, Baltimore, Maryland;
[†]Department of Chemical and Biomedical Engineering, Florida A&M University−Florida State University College of Engineering, Tallahassee, Florida; [‡]Department of Otolaryngology−Head and Neck Surgery, Johns Hopkins University School of Medicine, Baltimore, Maryland; [§]Department of Orthopedic Surgery, Johns Hopkins University School of Medicine, Baltimore, Maryland; [‖]Harvard Combined Orthopaedic Residency Program, Harvard Medical School, Boston, Massachusetts;
[¶]Department of Biomedical Engineering, Johns Hopkins University School of Medicine, Baltimore, Maryland; [#]Department of Neurosurgery, Mayo Clinic, Rochester, Minnesota; **Department of Radiation Oncology and Molecular Radiation Sciences, Johns Hopkins University School of Medicine, Baltimore, Maryland; and [††]Department of Mechanical Engineering, Whiting School of Engineering, Johns Hopkins University, Baltimore, Maryland

Purpose: Vertebral compression fracture is a common complication of spinal stereotactic body radiation therapy. Development of an in vivo model is crucial to fully understand how focal radiation treatment affects vertebral integrity and biology at

various dose fractionation regimens. We present a clinically relevant animal model to analyze the effects of localized, high-dose radiation on vertebral microstructure and mechanical integrity. Using this model, we test the hypothesis that fractionation of radiation dosing can reduce focused radiation therapy's harmful effects on the spine.

Methods and Materials: The L5 vertebra of New Zealand white rabbits was treated with either a 24-Gy single dose of focused radiation or 3 fractionated 8-Gy doses over 3 consecutive days via the Small Animal Radiation Research Platform. Nonirradiated rabbits were used as controls. Rabbits were euthanized 6 months after irradiation, and their lumbar vertebrae were harvested for radiologic, histologic, and biomechanical testing.

Results: Localized single-dose radiation led to decreased vertebral bone volume and trabecular number and a subsequent increase in trabecular spacing and thickness at L5. Hypofractionation of the radiation dose similarly led to reduced trabecular number and increased trabecular spacing and thickness, yet it preserved normalized bone volume. Single-dose irradiated vertebrae displayed lower fracture loads and stiffness compared with those receiving hypofractionated irradiation and with controls. The hypofractionated and control groups exhibited similar fracture load and stiffness. For all vertebral samples, bone volume, trabecular number, and trabecular spacing were correlated with fracture loads and Young's modulus ($P < .05$). Hypocellularity was observed in the bone marrow of both irradiated groups, but osteogenic features were conserved in only the hypofractionated group.

Conclusions: Single-dose focal irradiation showed greater detrimental effects than hypofractionation on the microarchitectural, cellular, and biomechanical characteristics of irradiated vertebral bodies. Correlation between radiologic measurements and biomechanical properties supported the reliability of this animal model of radiation-induced vertebral compression fracture, a finding that can be applied to future studies of preventative measures. © 2021 Elsevier Inc. All rights reserved.

Introduction

The spine is the most frequent site of bone metastasis, with 30% of cancer patients developing symptomatic spinal lesions during the course of their illness.[1] Advances in cancer surveillance, diagnostics, and therapeutics have prolonged life expectancy around the world, resulting in the conjoined rise in prevalence of spine metastases.[2,3] Similarly, the treatment armamentarium for spinal tumors has evolved rapidly in recent decades, with radiation therapy and surgery being the main modalities.

Stereotactic body radiation therapy (SBRT) is increasingly being used in the management of spinal metastases, owing to its far less invasive nature compared with surgery and its excellent local control.[4] SBRT uses the precise and accurate delivery of radiation for dose escalation to regions of gross and microscopic disease while continuing to meet dose constraints to the adjacent normal tissue, allowing delivery of higher biologically equivalent doses than conventional RT. However, vertebral compression fracture (VCF) is a well-established complication, reported in as many as 39% of patients treated with spinal SBRT.[26] Even conservative radiation doses are associated with an approximate fracture risk of 10%, and the majority of fractures occur within the first 4 months after SBRT.[5] This is highly problematic because it often necessitates invasive interventions such as cement augmentation or surgical stabilization in a patient population that often has a limited life expectancy. The mechanisms underlying VCF are believed to be related to those leading to tumor cell death, including development of osteoradionecrosis.[6]

Although a few studies have evaluated clinical, dosimetric, and radiographic risk factors that are predictive of VCF,[7-9] there are limited preclinical data exploring the effects of SBRT on vertebral integrity. Furthermore, there have been few preclinical studies exploring whether there is a significant advantage to using hypofractionated treatments as opposed to a single-dose treatment in regard to VCF risk. Development of an in vivo irradiation model is imperative to provide insight into the effects of radiation treatment on the incidence of VCF, potentially leading to changes in the standard of care for patients. Such a model will also allow testing of potential interventions to mitigate the risk of radiation-induced VCF in a much safer and cost-effective manner than clinical trials. For that purpose, we aimed to develop a clinically relevant animal model to analyze the effects of localized, high-dose radiation on vertebral microstructure and mechanical integrity, using the Small Animal Radiation Research Platform (Xstrahl Inc, Suwanee, Georgia).[10]

Methods

Study animals

To design, analyze, and report the present research study, the Animal Research: Reporting of In Vivo Experiments guidelines[11] were implemented. Skeletally mature male New Zealand white rabbits (Robinson Services Inc, Mocksville, North Carolina) weighing 2 kg to 5 kg were used for this study. Animals were housed in standard facilities and allowed to eat and drink ad libitum, and their conditions were monitored daily. All animals were handled following the policies and guidelines of our institutional animal care and use committee. The sample size was calculated using G*Power software (Heinrich-Heine-Universität Düsseldorf,

Düsseldorf, Germany), version 3.1.9.2,[12] with the following input parameters: effect size, 0.5; α error probability, 0.05; and power ($1 - \beta$ error probability), 0.8.

Anesthesia

Before irradiation, rabbits were weighed, and anesthesia was induced via an intramuscular injection of 0.7 mL of a solution containing ketamine hydrochloride (20-40 mg/kg) and xylazine (1-3 mg/kg). Once anesthetized, the rabbit's heart rate and breathing rate were monitored every 10 to 15 minutes to ensure that an adequate anesthesia depth was maintained for the duration of the irradiation session. Once irradiation was completed, the animal was monitored until fully alert and ambulatory. The rabbits were monitored daily for 3 consecutive days after irradiation to monitor for any signs of radiation-induced morbidity and then followed weekly until the time of sacrifice.

Irradiation protocol

After anesthesia of each rabbit, the paw-pinch test was performed to determine the level of sedation. The dorsal lumbar region was shaved to allow the identification via palpation of the L5 spinous process. L5 was chosen as the radiation target owing to its balance between vertebra size and accessibility for a clearer margin of radiation delivery. Once L5 was identified and marked, rabbits were positioned within a padded acrylic tube to maintain an upright position, exposing the lumbar region. Rabbits were then placed inside the Small Animal Radiation Research Platform to administer the radiation treatment. In all cases, the L5 vertebra was located using preliminary x-ray imaging (65 kVp, 0.9-1.4 mA). Briefly, an open field x-ray image was acquired to visualize the lumbar region and identify L5. Using a customized collimator of 6 cm by 6 cm, an additional x-ray image was obtained to verify the beam location. Then the same collimator was used to apply a radiation beam (single anterior-posterior beam) on that spinal level. According to the radiation protocol applied (220 kVp, 13 mA), 27 rabbits were divided into 3 experimental groups: (1) single 24-Gy dose (6 rabbits), (2) hypofractionated 8-Gy doses on 3 consecutive days (10 rabbits), and (3) nonirradiated control (11 rabbits). Rabbits were monitored as described and then euthanized 6 months after irradiation, and their lumbar vertebrae were harvested for radiologic and biomechanical testing.

Bone morphologic analysis

For microstructural analysis, excised L2 and L5 vertebral bodies (VBs) were imaged via microcomputed tomography (μCT) (SkyScan 1172, Bruker, Kontich, Belgium) at a resolution of approximately 9 μm (80 kV, 124 μA). In addition to the nonirradiated control group, the L2 VB of each animal was used as an additional out-of-irradiated-field control for radiologic microstructural analysis. The μCT scans were analyzed to determine microarchitectural parameters in accordance with the recommendations of the American Society for Bone and Mineral Research,[13] including bone volume divided by total volume (BV/TV [%]), trabecular thickness (μm), trabecular number (1/mm), and trabecular spacing (porosity) (μm).

Biomechanical testing

After μCT analysis, the L5 VBs were stored in a freezer at $-80°$C until mechanical tests were performed. Before testing, representative L5 VBs were thawed, and all the adhered soft tissue was meticulously removed. For each L5 VB, the bony endplates were partially embedded in cylindrical polymethyl methacrylate blocks (Coe Tray Plastic Fast Set, GC America Inc, Chicago, IL), poured within 25.4 mm by 5 mm (outer diameter × height) thin-walled acrylic tube potting molds.[14] Special attention was paid to obtain parallel surfaces between the superior and inferior sides of the potting blocks and a VB vector at an angle of 90° from the horizontal. Steps of this process are illustrated in Figure 1. The potted VBs were then measured for dimensions and tested destructively using an MTS Criterion Series 40 Material Test System (MTS, Eden Prairie, MN). Samples were placed on the stationary testing podium, and the 5kN compressive load cell was then lowered to barely contact the sample before compressive testing. The load cell was then lowered at a constant rate of 0.2 mm/s to apply compressive force until the point of sample failure. Data from the test were used to determine the vertebral fracture load (N), stiffness (EI), and Young's modulus (E [MPa or N•m^2]).

Histologic analysis

Representative L5 VBs were fixed in 4% paraformaldehyde overnight, decalcified in ethylene diamine tetraacetic acid (Sigma-Aldrich, St Louis, MO) for 2 weeks, dehydrated by ethanol series (70%, 95%, and 100%), and embedded in paraffin. Each block was sliced into 10-μm−thick axial sections at the center of the VBs. Slides were subsequently deparaffinized in xylene and rehydrated in a descending ethanol series (100%, 95%, and 70%). Hematoxylin and eosin (H&E) staining and Masson trichrome staining were conducted to evaluate the characteristics of the cortical and trabecular bone. Slides were analyzed at 2.5 ×, 10 ×, and 20 × magnification, and images were obtained using an Axio Observer Z1 microscope (Carl Zeiss AG, Oberkochen, Germany). Bone histomorphometric parameters (the number of empty osteocyte lacunae per bone area (EL per BA) [N.Lc/B.Ar], the total number of osteocyte lacunae per bone area (lucanae per BA) [N.Emp.Lc/B.Ar], and the percentage of empty osteocyte lacunae per total lacunae (EL per TL) [N.Emp.Lc/N.Lc]) were analyzed with ImageJ software (National Institutes of Health, Bethesda, MD) using 20 × -magnified H&E images. From each representative slice, 5 square areas (0.3 mm × 0.3 mm) were randomly
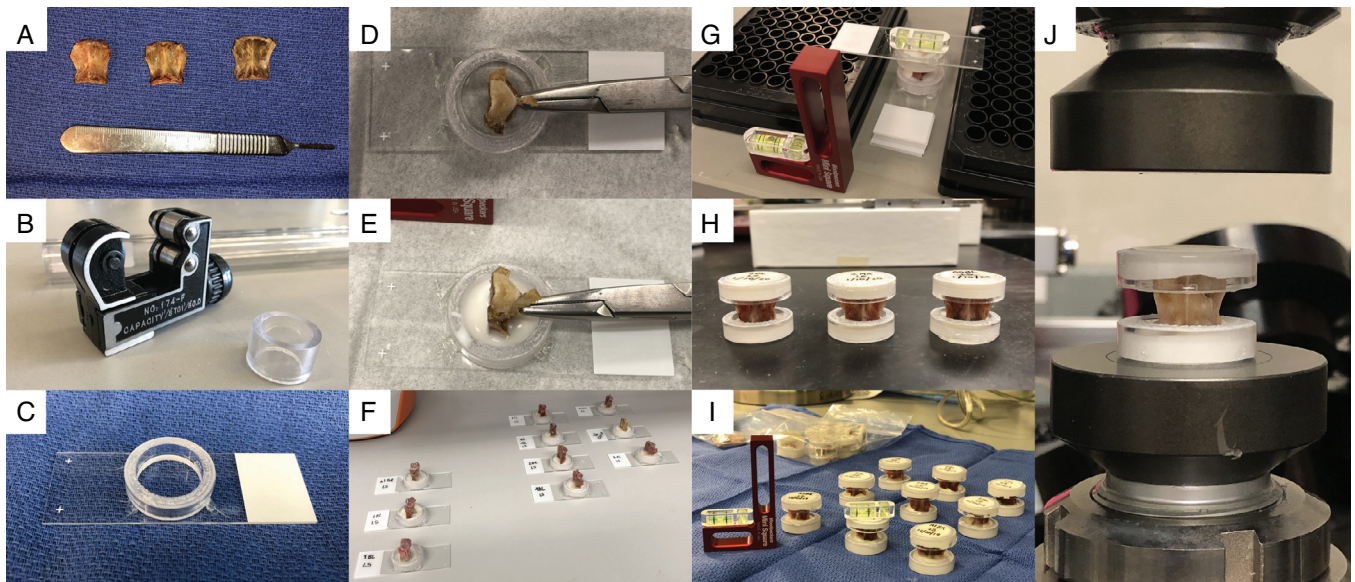
Fig. 1. Processing of vertebral body (VB) biomechanical testing. After harvesting of spines, L5 vertebrae were isolated. The posterior arch of each vertebra was carefully removed by cutting through the pedicles using an electric saw. (A) Each L5 VB was cleaned up, pulling out all the soft tissue including muscles, ligaments, and remaining cartilage on the endplates. (B) Using a tube cutter, thin-walled acrylic rings (outer diameter: 25.4 mm; height: 5 mm) were customized from a longer cylindrical acrylic tube. (C) Individually, acrylic rings were placed and partially fixed with high-temperature silicone glue on a glass microscope slide. (D) Each VB was positioned at an angle of 90° from the horizontal plane. A needle holder helped to keep VBs in a standing position during the initial embedding of the inferior endplate. (E) Polymethyl methacrylate was poured into the acrylic rings to partially embed the inferior endplates, and (F) then let solidify for 1 hour. Posteriorly, the samples were inverted, and the process was repeated to embed the superior endplates. (G, H, I) A miniature square and small bubble levelers were used during positioning and embedding of the samples to preserve the 90° angle of the vector and achieve an adequate alignment between both the superior and inferior rings. (J) Finally, the potted VBs were measured for dimensions and placed on the biomechanical tester podium to be compressed.

selected for quantification, and the mean value of all the measurements was taken as the final value of each group. Only lacunae with no osteocytes inside were counted as empty lacunae.

Immunohistochemistry analysis

After the histologic assessment, paraffin blocks were additionally sliced into 10-μm−thick axial sections at the center of the VBs to immunostain for bone markers to determine changes in bone composition. Briefly, after dewaxing and rehydration, slides were immersed in 1% Tween-20 (Sigma-Aldrich, St. Louis, MO); then heat−induced antigen retrieval was performed in a steamer using Target Retrieval Solution (Agilent Technologies, Santa Clara, CA; S170084-2) for 45 minutes. Slides were rinsed in phosphate-buffered saline solution, endogenous peroxidase and phosphatase were blocked (Agilent Technologies, Santa Clara, CA; S2003), and sections were then incubated with 1 of the following primary antibodies: antiosteocalcin monoclonal antibody (Sigma-Aldrich, St. Louis, MO; MABD123, 1:100 dilution), anticollagen type I (Abcam, Cambridge, UK; AB88147, 1:400 dilution), or antialkaline phosphatase (Fisher Scientific, Waltham, MA; NB1002637, 1:400 dilution) for 45 minutes at room temperature. The primary antibodies were detected by 30-minute incubation with horseradish peroxidase-labeled antimouse secondary antibody (Leica Microsystems, Wetzlar, Germany; PV6114) followed by detection with 3,3′−diaminobenzidine (Sigma-Aldrich, St. Louis, MO; D4293), counterstaining with Mayer hematoxylin, dehydration, and mounting.

Statistical analysis

Comparisons of means of continuous variables were performed between the irradiated groups and the control group via 2-tailed unpaired t tests. The Pearson correlation coefficient, r, with a 95% confidence interval, was used to evaluate the linear correlation between μCT measurements and biomechanical testing data. A P value <.05 was considered statistically significant for all comparisons. GraphPad Prism, version 9.0 (GraphPad Software, La Jolla, CA), was used for all statistical analyses.
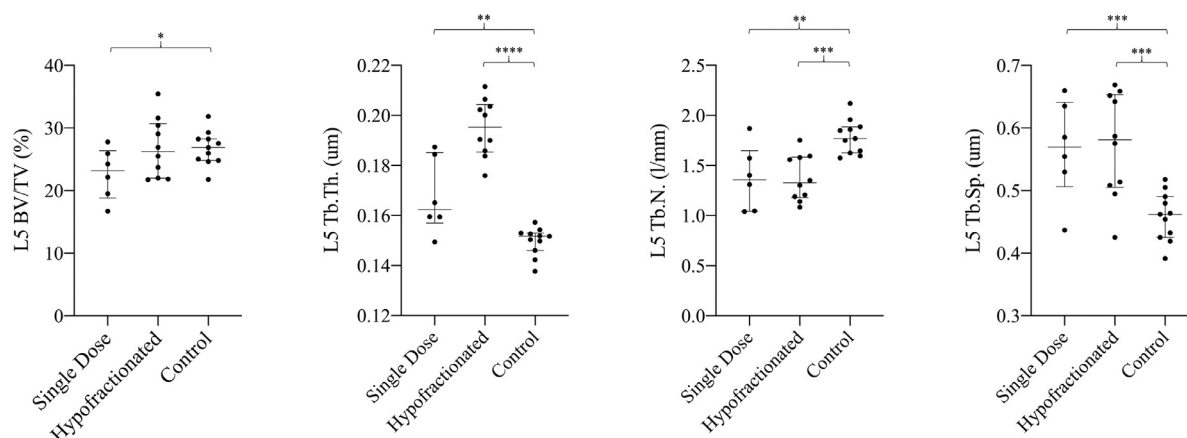
Fig. 2. Scatter plots of computed tomography microarchitectural measurements of L5 vertebral bodies. In the comparisons between experimental and control groups via *t* tests, structural trabecular changes were observed in the irradiated groups, and they were more evident in the samples receiving a high dose in a single dose. The struts of the trabeculae were also thicker in the irradiated groups. The increase in bone thickness was more notable in the hypofractionated group, which could explain in part why hypofractionation displayed a bone volume/total volume ratio not significantly different from controls. * = $P < .05$; **$P < .01$; ***$P < .001$; ****$P < .0001$.

Results

Radiation led to dose fractionation-dependent changes in CT vertebral bone volume and microarchitectural features

Trabecular bone microarchitectural measurements of L5 VBs for all experimental groups are presented in Figure 2. The hypofractionated and control groups showed significantly higher mean BV/TV values, $26.8 \pm 4.7\%$ and $26.7 \pm 2.7\%$, respectively, than that obtained in the single-dose group ($22.7 \pm 4.1\%$). Intergroup comparisons revealed that the difference between the single-dose and control-group BV/TV values was statistically significant ($P = .02$), whereas the difference between the hypofractionated group and control group was not significant. Mean trabecular thickness was highest in the hypofractionated group at 0.19 ± 0.01 μm, followed by the single-dose group at 0.16 ± 0.01 μm and the control group at 0.14 ± 0.00 μm; multiple comparisons revealed that these differences were statistically significant ($P < .001$).

The control group showed the highest mean trabecular number at 1.78 ± 0.16 1/mm, compared with 1.37 ± 0.31 1/mm in the single-dose group and 1.37 ± 0.22 1/mm in the hypofractionated group. Comparison of trabecular number values between the control group and either the single-dose or hypofractionated group were statistically significant ($P = .003$ and $P < .001$, respectively). Mean trabecular spacing values were significantly higher among the irradiated groups at 0.57 ± 0.08 μm for the hypofractionated group and 0.56 ± 0.08 μm for the single-dose group, compared with the control group at 0.45 ± 0.03 μm ($P < .001$ and $P = .001$, respectively).

Unlike the significant difference in trabecular thickness values, the differences in BV/TV, trabecular number, and trabecular spacing between the single-dose and hypofractionated groups were not statistically significant. In addition to microarchitectural differences in trabecular bone, an apparent increase in cortical bone shell thickness was observed in the hypofractionated group on CT images, although this was not measured quantitatively. Furthermore, no differences were found among microarchitectural parameters of L2 VBs, except for the trabecular thickness between the hypofractionated and control groups; however, this difference was lower than in L5 VBs (Supplemental Figure E1).

Single-dose irradiation caused detrimental effects on biomechanical properties to a greater extent than hypofractionation

Potted VB sample fracture loads, stiffnesses, and Young's modulus values are summarized in Supplemental Table E1. Height, width, and cross-sectional sample areas were similar among groups, with no significant differences. Single-dose irradiated samples tended to show lower mean fracture loads and stiffness compared with those receiving hypofractionated irradiation and the nonirradiated controls. The mean fracture load value for the single-dose group was 1327 ± 769.6 N; for the hypofractionated group, 2259 ± 442.7 N; and for the control group, 2126 ± 107.7 N. The mean Young's modulus value for the single-dose group was 862.1 ± 261.5 MPa; for the hypofractionated group, 1009 ± 167.9 MPa; and for the control group, 1018 ± 136.7 MPa. Interestingly, hypofractionated and control groups exhibited similar means for fracture load and stiffness.

Results of linear regression analyses, which were performed to determine whether there were correlations between trabecular bone microarchitectural properties and biomechanical testing measurements, are summarized in
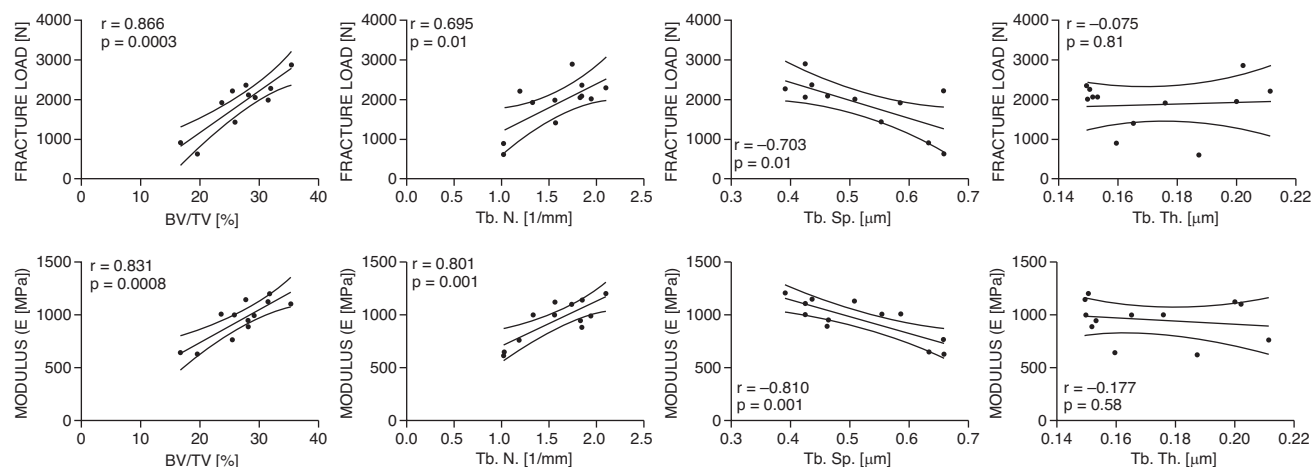
Fig. 3. Correlation of biomechanical and microarchitectural properties. Using Pearson r, the fracture load (upper graphs) and Young modulus (lower graphs) were found to correlate positively with the bone volume/total volume ratio and trabecular number across all the samples; in other words, the greater the bone volume and number of trabecular struts, the higher stiffness and greater force required to fracture. Inversely, both mechanical outcomes were negatively correlated with trabecular spacing; thus, the greater the trabecular spacing or porosity of the sample, the less stiffness and lower force needed to fracture. No significant correlation was found between the trabecular thickness of the samples and their mechanical performance. Individual r and P values are given in each graph, as well as best-fit lines and 95% confidence bands.

Figure 3. For all samples as a whole, BV/TV, trabecular number, and trabecular spacing were found to be significantly correlated both with fracture load and Young's modulus ($P < .05$).

Radiation decreased bone marrow cellularity while preserving bone healing with hypofractionation

The microarchitectural details (ie, trabecular bone thickness, number, and spacing) of irradiated and control vertebrae observed via H&E and Masson trichrome histologic staining were found to be consistent with those found via CT imaging measurements. A decreased quantity of trabecular struts was observed in the irradiated groups compared with the nonirradiated control group and was more evident in the single-dose group. Also, spacing between trabecular septa was wider in the single-dose and hypofractionated groups than in the control group. Moreover, irradiated groups displayed an increase in thickness of the trabeculae, but only the hypofractionated group exhibited an increase in the thickness of the cortical shell.

In addition to the trabecular microarchitectural differences, irradiated groups exhibited trabecular and bone marrow hypocellularity compared with the nonirradiated group. This deleterious radiation effect was more pronounced in the single-dose group, which showed an increased number of empty lacunae and the disappearance of ossification centers and their bone matrices. Interestingly, these ossification centers were not only preserved in the hypofractionated group but were also active with an increased number of haversian systems at their surrounding area (see Fig. 4). In the quantification of empty osteocyte lacunae, the N.Emp.

Lc/B.Ar and N.Emp.Lc/N.Lc were significantly higher in the single-dose and hypofractionated groups than in the control group. The single-dose group displayed the highest mean N.Emp.Lc/B.Ar at $273.7/\text{mm}^2 \pm 53.1/\text{mm}^2$, compared with $88.3/\text{mm}^2 \pm 48.5/\text{mm}^2$ and $38.4/\text{mm}^2 \pm 40.1/\text{mm}^2$ in the hypofractionated and the single-dose group, respectively. The mean N.Emp.Lc/N.Lc percentages were significantly higher among the irradiated groups at 39.5% $\pm$ 7.1% for the single-dose group and 12.4% $\pm$ 5.9% for the hypofractionated group, compared with the control group at 5.0% $\pm$ 4.7% ($P < .001$ and $P = .003$, respectively). There was no significant difference in the mean values of total N.Lc/B.Ar between groups (see Fig. 5).

Trabeculae from the hypofractionated and control groups diffusely expressed antiosteocalcin across most of the trabecular struts and trabecular bone marrow, whereas expression of anticollagen type I was observed only in the trabecular struts in both groups. Discrete granular dot-like expression of antialkaline phosphatase was seen in proximity to the ossification centers in the hypofractionated and control groups. Expression of those osteoblastic markers in the single-dose group was negligible (see Fig. 6).

Discussion

With the life expectancy of cancer patients rising worldwide, the prevalence of spinal metastases is increasing.[2,15] Given that half of cancer patients will develop spinal metastasis[3] and the superiority of high-precision radiation therapy compared with conventional RT for treating painful spine lesions,[16] increased use of SBRT is expected, which may lead to a surge in the incidence of VCF. VCF significantly
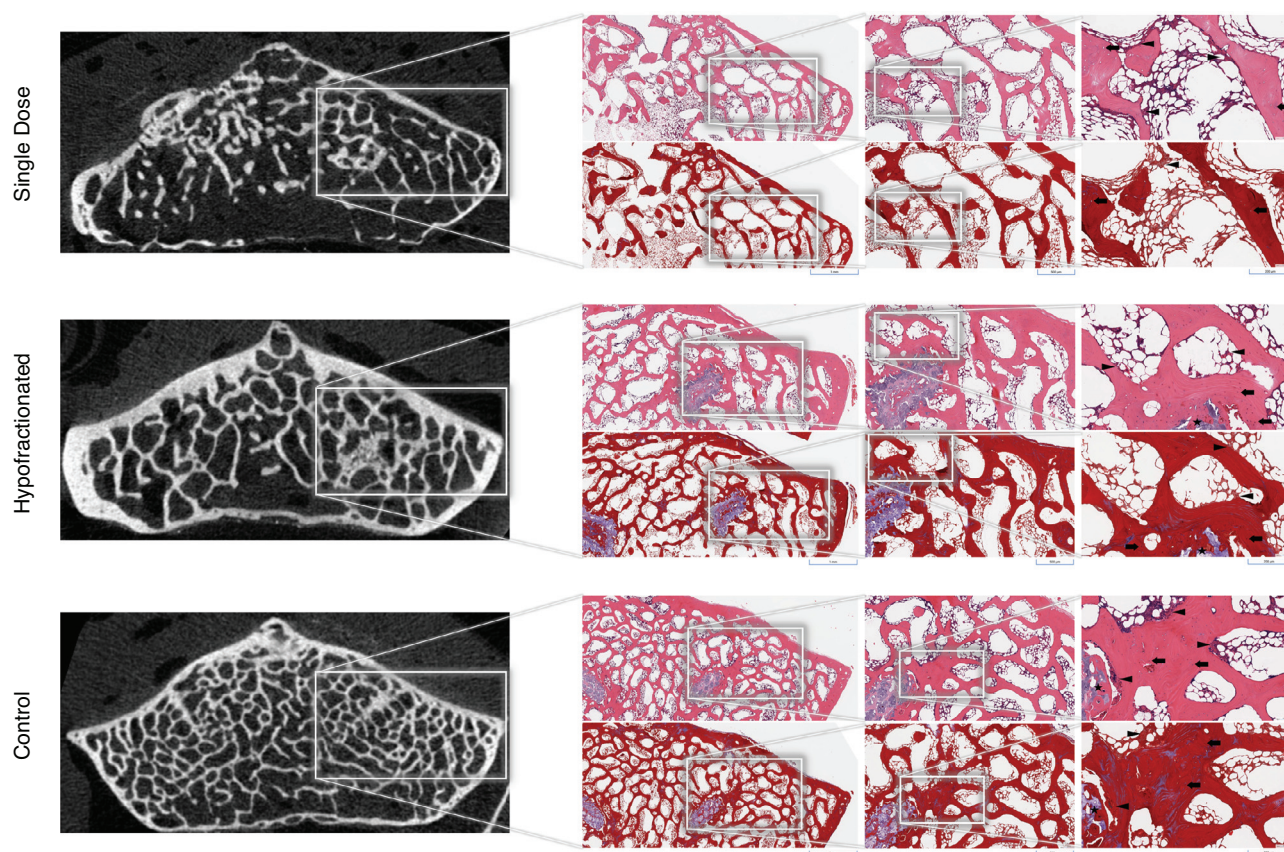
Fig. 4. Histologic analysis. Representative photographs of sections of vertebral bodies stained with hematoxylin and eosin (upper series) and Masson trichrome (lower series) staining at 2 × (left), 4 × (center), and 10 × (right) magnification. The delivery of high radiation in a single dose caused significant porosity and loss of trabecular struts and bone and bone marrow cellularity. An increase of empty lacunae (single-dose, arrows) along with hypocellular, fibrotic bone marrow (single-dose, arrow heads) was observed. Although dose fractionation also caused porosity and loss of trabeculae, there was increased thickness of both the trabecular centrum and the cortical shell bone. Also, bone marrow hypocellularity and fibrosis (hypo-fractionated, arrow heads) were present, but trabecular cellularity (hypofractionated, arrows) was mostly preserved. Increased osteogenic centers and surrounding haversian systems were identified (hypofractionated, star). Nonirradiated controls displayed osteogenic centers (control, star) and a normal trabecular structure and cellularity, both in the trabeculae (control, arrow) and bone marrow (control, arrow heads). Histologic findings were found to be consistent with those observed on representative computed tomography imaging (far left).

affects patient quality of life owing to significant pain, neurologic deficits, and the risk of subsequent invasive and surgical interventions.[7,17] For that reason, many clinical studies have focused on identifying predictive factors (ie, the dose per fraction and spinal instability neoplastic scoring criteria[18]) associated with the development of radiation-induced VCF.[7] However, few preclinical studies have examined the effects of radiation on vertebral structure and mechanical properties. To our knowledge, we report the first study using a specifically designed animal model to better understand how localized radiation leads to vertebral changes that ultimately cause fractures.

Although most knowledge regarding radiation-induced VCF comes from clinical studies,[5,17,19-31] animal models offer numerous advantages, including a wider range of testable radiation regimens, the capacity to analyze longitudinal vertebral biomechanical and cellular behavior in detail

and over time, the ability to distinguish the degree of bone structural damage by radiation independently of tumor histology, and the potential to evaluate various treatments. Although a limited number of animal studies to date have researched the effects of various modalities of radiation delivery on the spine, the majority have investigated the effects of radiation on bone growth,[32-35] tumor induction,[36] or spinal fusion outcomes,[37,38] and none of those have centered their attention on VCFs secondary to localized x-ray delivery at SBRT-relevant radiation doses. In this study, we report the results of an animal model for focal radiation-induced VCF, describing the dose fractionation−dependent effects on vertebral microarchitectural and biomechanical characteristics. Although rat and mouse models are more commonly used to study the effects of radiation on bone, we used rabbits because they exhibit more dynamic and representational similarities to humans and are thus more
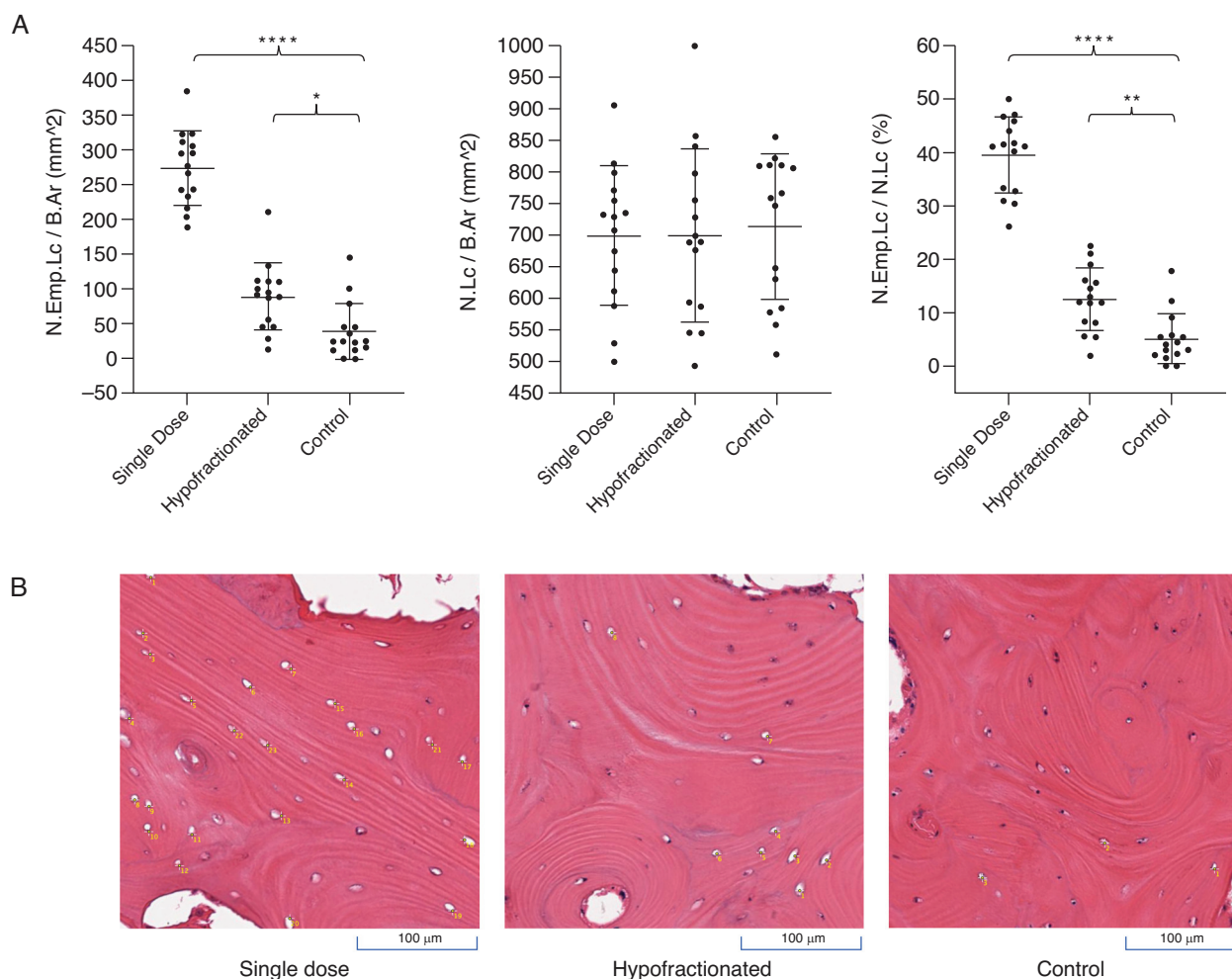
Fig. 5.   Quantification of empty osteocyte lacunae. (A) Scatter plots of histomorphometric analysis of N.Emp.Lc/B.Ar (left), N.Lc/B.Ar (center), and N.Emp.Lc/N.Lc (right). Multiple comparisons between groups showed a significant difference in N. Emp.Lc/B.Ar and N.Emp.Lc/N.Lc between the irradiation groups compared with the control group. These values were substantially higher in the group treated with a high dose in a single dose. All groups exhibited a similar total N.Lc/B.Ar. (B) For the quantification of empty lacunae, representative hematoxylin and eosin images in 20 × magnification (0.3 mm × 0.3 mm) were used. *$P < .05$; **$P < .01$; ****$P < .0001$. *Abbreviations:* N.Emp.Lc/B.Ar = total number of osteocyte lacuna per bone area; N.Emp.Lc/N.Lc = percentage of empty osteocyte lacuna per total lacunae; N.Lc/B.Ar = number of empty osteocyte lacuna per bone area.

clinically applicable.[39] This study's model observed that a single localized dose of 24 Gy radiation led to the loss of vertebral BV and decreased trabecular number and a subsequent increase in trabecular thickness and spacing. In contrast, radiation dose hypofractionation (24 Gy delivered in 3 fractions of 8 Gy) similarly led to a reduced trabecular number and increased trabecular thickness and spacing but preserved normalized BV. Single-fraction treatment also lowered stiffness and induced VCF at a lower load compared with hypofractionation. Radiation-induced changes in bone microarchitecture among the groups were correlated significantly with fracture loads and Young's modulus. Furthermore, although bone marrow hypocellularity was seen in both single and hypofractionated doses, only hypofractionation preserved osteogenic features.

One aspect of SBRT for spinal metastasis that requires further investigation is the relationship between dose fractionation and volume and radiation-induced complications. The heterogeneity of dose fractionation and target-volume delineation regimens among clinical studies has hindered the ability to reach a consensus on the optimal balance between radiation dose and number of fractions[40] to maximize local control while minimizing toxicity. Nevertheless, high dose-per-fraction SBRT[7] and a larger target volume[9] have already been identified as significant risk factors for VCF. For instance, in a retrospective cohort study of 167 spinal segments treated with spine SBRT, Cunha et al[21] observed an increased risk of fracture in segments receiving ≥20 Gy per fraction. In a multi-institutional study, the same research group not only confirmed this threshold of 20 Gy
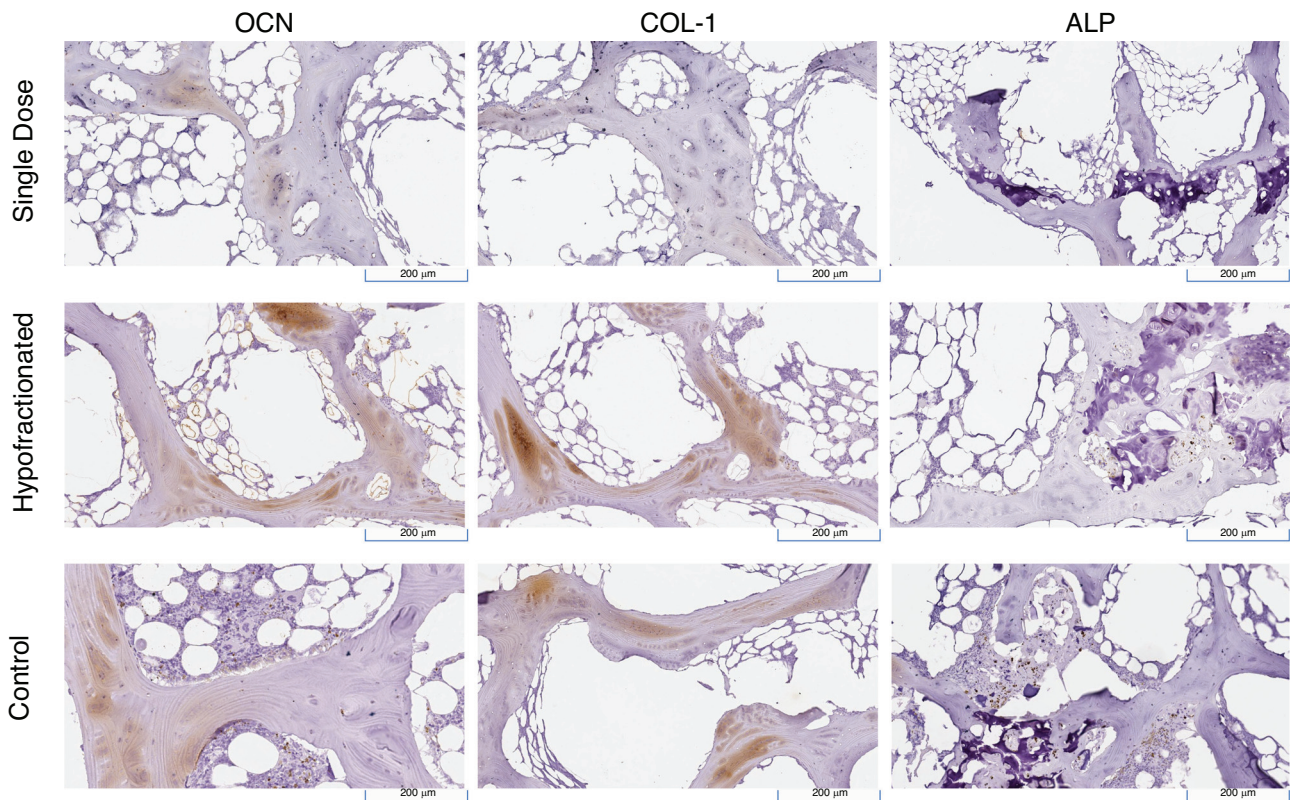
Fig. 6. Immunohistochemistry for bone proteins. Representative photographs of sections of vertebral bodies stained for bone markers showed a decrease in the expression of antiosteocalcin, anticollagen type I, and antialkaline phosphatase after delivery of high radiation in a single fraction. Expression of these osteoblastic markers did not seem to vary significantly from nonirradiated controls.

but also stratified the risk of VCF in subgroups based on dose per fraction.[5] After stratification, the 39% cumulative incidence of VCF they found at 1 year in patients treated with 24 Gy in a single fraction matched the findings of a previous study by Rose et al,[26] which had reported a VCF rate of 39% with high-dose single-fraction SBRT (single-dose treatment at 24 Gy). In addition to the prescription dose, the volume of the irradiated spine also may be critical for determining VCF risk. Recently, Chen et al[9] observed, using a novel normal-tissue complication probability analysis, that larger spinal volumes receiving low to intermediate radiation doses (D80% and D50%) were more strongly associated with VCF than small, high-dose areas. Therefore, the reduction of post-SBRT VCF may require both dosimetric optimization and minimization of the target volume. With this study's animal model, we focused on the study of the dose fractionation as a VCF risk factor. Consistent with studies reporting an increased VCF risk threshold of ≥20 Gy per fraction,[5,21] in the current study's irradiation model, the delivery of 24 Gy in a single fraction caused harmful changes in the cancellous bone to a greater extent than 3 fractions of 8 Gy each. In single-dose−irradiated VBs, the decreased BV/TV and trabecular number and the increased trabecular spacing likely explain the observed lower fracture threshold. Although hypofractionated VBs also showed structural changes, the preservation of bone

volume and the increased trabecular bone thickness correlated with the improved biomechanical performance of this group, which was similar to that of nonirradiated controls.

Besides detecting microarchitectural differences, identifying variations of the biomechanical properties across the different radiation treatments was also crucial for this study. It allowed us to verify that our radiation-induced VCF model accurately replicates what is seen in patients receiving SBRT. Besides confirming that the delivery of 24 Gy in a single dose fosters a greater decrease in fracture load and Young's modulus than does hypofractionation, we corroborated a significant correlation between biomechanical measurements and specific CT microarchitectural features such as BV/TV, trabecular number, and trabecular spacing. Some other animal models have previously described this relationship between bone microarchitecture and mechanical properties after radiation. For instance, Soares et al[41] reported a decrease of normal anisotropy on the microarchitecture of cortical bone and an increase in bone fragility in rabbits after delivery of a single radiation dose of 30 Gy. Although their study focused on the effects of radiation on the properties of tibial cortical bone and this study examined the postirradiation changes in vertebral trabecular bone, this study's single-dose group results shared similarities with the findings of Soares et al. In another example, this one in a spine model, Alwood et al[42] also reported

changes in vertebral microarchitecture and mechanical properties in mice 1 month after receiving a spaceflight-relevant radiation dose (heavy ion [^{56}Fe] irradiation at a 2-Gy dose). They found that irradiation decreased vertebral trabecular BV/TV and trabecular number while increasing trabecular spacing, effects that we also observed in our single-dose group. Furthermore, Alwood et al found that irradiated vertebrae developed a thicker cortical shell and greater cross-sectional cortical bone area, a finding that we also recognized in this study's hypofractionated group and that we believe may explain in part the maintenance of fracture load and stiffness values in the hypofractionated group compared with the single-dose group.

Corroborating this study's CT microarchitectural findings, we observed histologic evidence of radiation-attributed microscopic changes that varied depending on the dose fractionation. Whereas bone tissue that received 24 Gy in a single dose was characterized by evident toxic effects, including bone marrow and trabecular bone hypocellularity as well as increased numbers of empty lacunae and porosity, bone receiving hypofractionated radiation developed less obvious radiotoxicity changes and also seemed to have preserved osteogenic capabilities, a finding supported by the expression of bone-specific proteins. Some of these observations were consistent with a previous report by Al-Omair et al,[43] which described histopathologic analyses of VCF in 2 spinal stereotactic radiosurgery cases. One patient received 20 Gy in a single dose, whereas the other was treated with 24 Gy in 2 fractions. Biopsies indicated avital bone and necrotic debris in the single-dose case and dense fibrous tissue with local lymphocytic inflammation in the fractionated case. Although we also observed avital bone and fibrous tissue in this study's single-dose and hypofractionated groups, respectively, we found less necrotic debris, fibrous tissue, and lymphocytic infiltration than in the clinical cases. We hypothesize that our shorter postradiation window (6 months vs ≥1 year) and lack of a tumoral component may explain these differences.

Even though our model is a close representation of this clinically relevant problem, this study was not exempt from limitations. One limitation is that 24 Gy in a single dose is a substantially different biologically effective dose than 24 Gy delivered in 3 fractions. It is, therefore, possible that the observed vertebral differences are reflective of a lower dose rather than fractionation; however, retrospective data suggest excellent local tumor control across fractionation regimens, including 24 Gy in 3 fractions, which suggests that our hypofractionated dose is still clinically effective even if it does represent a lower biologically effective dose. Although we believe that the study design is appropriate for an initial establishment of this model, further investigation of additional radiation dose fractionation schedules with analysis at different postradiation time points is needed. This would allow us to better quantify the extent to which dose fractionation may be used to limit VCF risk, identify the timeline of biological bone changes after treatment, and determine the appropriate timing for implementing interventions to prevent radiation-induced complications.

Conclusions

In this in vivo localized spinal irradiation model, single-dose delivery of 24 Gy was more harmful to vertebral body microarchitectural, cellular, and biomechanical properties than hypofractionation of the same radiation dose. Although hypofractionation also caused adverse effects, we observed structural and histologic changes suggesting preservation of bone regeneration capacity. Those findings, along with significant correlation between radiologic measurements and biomechanical properties, support the reliability of this animal model for radiation-induced VCF. Most importantly, this model will enable future studies of VCF preventative measures and interventions in a safe and cost-effective manner.

References

1. Wu AS, Fourney DR. Evolution of treatment for metastatic spine disease. *Neurosurg Clin N Am* 2004;15(4):401–411.
2. Allemani C, Matsuda T, Di Carlo V, et al. Global surveillance of trends in cancer survival 2000-14 (CONCORD-3): Analysis of individual records for 37 513 025 patients diagnosed with one of 18 cancers from 322 population-based registries in 71 countries. *Lancet* 2018;391(10125):1023–1075.
3. Chen Y, He Y, Zhao C, Li X, Zhou C, Hirsch FR. Treatment of spine metastases in cancer: A review. *J Int Med Res* 2019 300060519888107.
4. Kumar N, Malhotra R, Zaw AS, et al. Evolution in treatment strategy for metastatic spine disease: Presently evolving modalities. *Eur J Surg Oncol* 2017;43(9):1784–1801.
5. Sahgal A, Atenafu EG, Chao S, et al. Vertebral compression fracture after spine stereotactic body radiotherapy: A multi-institutional analysis with a focus on radiation dose and the spinal instability neoplastic score. *J Clin Oncol* 2013;31(27):3426–3431.
6. Osborn VW, Lee A, Yamada Y. Stereotactic body radiation therapy for spinal malignancies. *Technol Cancer Res Treat* 2018;17 1533033818802304.
7. Faruqi S, Tseng CL, Whyne C, et al. Vertebral compression fracture after spine stereotactic body radiation therapy: A review of the pathophysiology and risk factors. *Neurosurgery* 2018;83 (3):314–322.
8. Ehresman J, Schilling A, Pennington Z, et al. A novel MRI-based score assessing trabecular bone quality to predict vertebral compression fractures in patients with spinal metastasis. *J Neurosurg Spine* 2019;1–8.
9. Chen X, Gui C, Grimm J, et al. Normal tissue complication probability of vertebral compression fracture after stereotactic body radiotherapy for de novo spine metastasis. *Radiother Oncol* 2020;150:142–149.
10. Tryggestad E, Armour M, Iordachita I, Verhaegen F, Wong JW. A comprehensive system for dosimetric commissioning and Monte Carlo validation for the small animal radiation research platform. *Phys Med Biol* 2009;54(17):5341–5357.
11. Kilkenny C, Browne W, Cuthill IC, Emerson M, Altman DG, Group NCRRGW. Animal research: Reporting in vivo experiments: The ARRIVE guidelines. *J Gene Med* 2010;12(7):561–563.
12. Faul F, Erdfelder E, Buchner A, Lang AG. Statistical power analyses using G*Power 3.1: Tests for correlation and regression analyses. *Behav Res Methods* 2009;41(4):1149–1160.

13. Bouxsein ML, Boyd SK, Christiansen BA, Guldberg RE, Jepsen KJ, Muller R. Guidelines for assessment of bone microstructure in rodents using micro-computed tomography. *J Bone Miner Res* 2010;25(7):1468–1486.

14. Scheibler AG, Gotschi T, Widmer J, et al. Feasibility of the annulus fibrosus repair with in situ gelating hydrogels—A biomechanical study. *PLoS One* 2018;13(12) e0208460.

15. Glicksman RM, Tjong MC, WFP Neves-Junior, et al. Stereotactic ablative radiotherapy for the management of spinal metastases: A review. *JAMA Oncol* 2020;6(4):567–577.

16. Sahgal A, Myrehaug SD, Siva S, et al. CCTG SC.24/TROG 17.06: A randomized phase II/III study comparing 24Gy in 2 stereotactic body radiotherapy (SBRT) fractions versus 20Gy in 5 conventional pallia-tive radiotherapy (CRT) fractions for patients with painful spinal metastases. *Int J Radiat Oncol Biol Phys* 2020;108(5):1397–1398.

17. Boyce-Fappiano D, Elibe E, Schultz L, et al. Analysis of the factors contributing to vertebral compression fractures after spine stereotactic radiosurgery. *Int J Radiat Oncol Biol Phys* 2017;97(2):236–245.

18. Fisher CG, DiPaola CP, Ryken TC, et al. A novel classification system for spinal instability in neoplastic disease: An evidence-based approach and expert consensus from the Spine Oncology Study Group. *Spine (Phila Pa 1976)* 2010;35(22):E1221–E1229.

19. Boehling NS, Grosshans DR, Allen PK, et al. Vertebral compression fracture risk after stereotactic body radiotherapy for spinal metastases. *J Neurosurg Spine* 2012;16(4):379–386.

20. Chang JH, Shin JH, Yamada YJ, et al. Stereotactic body radiotherapy for spinal metastases: What are the risks and how do we minimize them? *Spine (Phila Pa 1976)*41S238–S245.

21. Cunha MV, Al-Omair A, Atenafu EG, et al. Vertebral compression fracture (VCF) after spine stereotactic body radiation therapy (SBRT): Analysis of predictive factors. *Int J Radiat Oncol Biol Phys* 2012;84(3):e343–e349.

22. Germano IM, Carai A, Pawha P, Blacksburg S, Lo YC, Green S. Clini-cal outcome of vertebral compression fracture after single fraction spine radiosurgery for spinal metastases. *Clin Exp Metastasis* 2016;33(2):143–149.

23. Jawad MS, Fahim DK, Gerszten PC, et al. Vertebral compression fractures after stereotactic body radiation therapy: A large, multi-institutional, multinational evaluation. *J Neurosurg Spine* 2016;24(6):928–936.

24. Lecouvet F, Richard F, Vande Berg B, et al. Long-term effects of localized spinal radiation therapy on vertebral fractures and focal lesions appearance in patients with multiple myeloma. *Br J Haematol* 1997;96(4):743–745.

25. Lee SH, Tatsui CE, Ghia AJ, et al. Can the spinal instability neoplastic score prior to spinal radiosurgery predict compression fractures fol-lowing stereotactic spinal radiosurgery for metastatic spinal tumor? A post hoc analysis of prospective phase II single-institution trials. *J Neurooncol* 2016;126(3):509–517.

26. Rose PS, Laufer I, Boland PJ, et al. Risk of fracture after single frac-tion image-guided intensity- modulated radiation therapy to spinal metastases. *J Clin Oncol* 2009;27(30):5075–5079.

27. Sharma M, Bennett EE, Rahmathulla G, et al. Impact of cervicothora-cic region stereotactic spine radiosurgery on adjacent organs at risk. *Neurosurg Focus* 2017;42(1):E14.

28. Thibault I, Al-Omair A, Masucci GL, et al. Spine stereotactic body radiotherapy for renal cell cancer spinal metastases: Analysis of out-comes and risk of vertebral compression fracture. *J Neurosurg Spine* 2014;21(5):711–718.

29. Thibault I, Whyne CM, Zhou S, et al. Volume of lytic vertebral body metastatic disease quantified using computed tomography-based image segmentation predicts fracture risk after spine stereotactic body radiation therapy. *Int J Radiat Oncol Biol Phys* 2017;97(1):75–81.

30. Virk MS, Han JE, Reiner AS, et al. Frequency of symptomatic verte-bral body compression fractures requiring intervention following sin-gle-fraction stereotactic radiosurgery for spinal metastases. *Neurosurg Focus* 2017;42(1):E8.

31. Sung SH, Chang UK. Evaluation of risk factors for vertebral compres-sion fracture after stereotactic radiosurgery in spinal tumor patients. *Korean J Spine* 2014;11(3):103–108.

32. Al-Hilli F, Wright EA. The short term effects of a supra-lethal dose of irradiation and changes in the environmental temperature on the growth of tail bones of the mouse. *Br J Exp Pathol* 1983;64(6):684–692.

33. Hartsell WF, Hanson WR, Conterato DJ, Hendrickson FR. Hyperfrac-tionation decreases the deleterious effects of conventional radiation fractionation on vertebral growth in animals. *Cancer* 1989;63(12):2452–2455.

34. Wechsler-Jentzsch K, Huepfel H, Schmidt W, Wandl E, Kahn B. Fail-ure of hyperfractionated radiotherapy to reduce bone growth arrest in rats. *Int J Radiat Oncol Biol Phys* 1993;26(3):427–431.

35. Urano M, Verhey LJ, Goitein M, et al. Relative biological effective-ness of modulated proton beams in various murine tissues. *Int J Radiat Oncol Biol Phys* 1984;10(4):509–514.

36. Ootsuyama A, Tanooka H. Induction of osteosarcomas in mouse lum-bar vertebrae by repeated external beta-irradiation. *Cancer Res* 1989;49(6):1562–1564.

37. Alanay A, Wang JC, Shamie AN, Napoli A, Chen C, Tsou P. A novel application of high-dose (50kGy) gamma irradiation for demineralized bone matrix: Effects on fusion rate in a rat spinal fusion model. *Spine J* 2008;8(5):789–795.

38. Bouchard JA, Koka A, Bensusan JS, Stevenson S, Emery SE. Effects of irradiation on posterior spinal fusions. A rabbit model. *Spine (Phila Pa 1976)* 1994;19(16):1836–1841.

39. Marmor MT, Dailey H, Marcucio R, Hunt AC. Biomedical research models in the science of fracture healing—Pitfalls & promises. *Injury* 2020;51(10):2118–2128.

40. De Bari B, Alongi F, Mortellaro G, Mazzola R, Schiappacasse L, Guckenberger M. Spinal metastases: Is stereotactic body radiation therapy supported by evidences? *Crit Rev Oncol Hematol* 2016;98:147–158.

41. Soares PBF, Soares CJ, Limirio P, et al. Effect of ionizing radiation after-therapy interval on bone: Histomorphometric and biomechanical characteristics. *Clin Oral Investig* 2019;23(6):2785–2793.

42. Alwood JS, Yumoto K, Mojarrab R, et al. Heavy ion irradiation and unloading effects on mouse lumbar vertebral microarchitecture, mechanical properties and tissue stresses. *Bone* 2010;47(2):248–255.

43. Al-Omair A, Smith R, Kiehl TR, et al. Radiation-induced vertebral compression fracture following spine stereotactic radiosurgery: Clini-copathological correlation. *J Neurosurg Spine* 2013;18(5):430–435.